American Mineralogist, Volume 87, pages 845–852, 2002

Structural properties and heat-induced oxidation-dehydrogenation of manganoan ilvaite from Perda Niedda mine, Sardinia, Italy

PAOLA BONAZZI* AND LUCA BINDI

Dipartimento di Scienze della Terra, Università di Firenze, Via La Pira 4, I-50121, Florence, Italy

ABSTRACT

An unusually Mn-rich ilvaite sample from the Perda Niedda mine in Sardinia, Italy, was studied in order to clarify the Mn^{2+} distribution among the different structural sites, and to observe the structural response of the mineral upon thermally induced oxidation-dehydrogenation. The crystal structure and the chemical composition of one crystal [a = 13.014(5), b = 8.867(3), c = 5.838(4) Å, β = 90.02(4)°] were investigated. X-ray crystal-structure refinement, performed in the *Pnam* space group, and electron microprobe analyses yielded the formula $(Ca_{0.98}Mn^{2+}_{0.02})(Fe^{3+}Fe^{2+})(Mn_{0.72}Fe^{2+}_{0.28})(Si_2O_7)O(OH)$. Crystal chemical details, compared to structural data from literature, led to the assumption that Mn^{2+} replaces Fe^{2+}, mainly at the M2 site. Annealing experiments and structure refinements were performed in the temperature range 400–690 °C. No phase transition was observed over the entire temperature range. Oxidation of Fe^{2+} at the M1 site, with concomitant dehydrogenation, was deduced from examination of the structural adjustments occurring as the temperature was increased. A useful model to evaluate a possible $OH^- \leftrightarrow O^{2-}$ substitution in ilvaite was obtained.

INTRODUCTION

Ilvaite, $CaFe^{2+}_2Fe^{3+}(Si_2O_7)O(OH)$, a mixed-valence iron sorosilicate, was considered to be orthorhombic (Belov and Mokeeva 1954; Beran and Bittner 1974; Haga and Takéuchi 1976) until Bartholomé et al. (1968) demonstrated the existence of a monoclinic phase (space group $P2_1/a$). Ilvaite undergoes a crystallographic phase transition between 60–117 °C (Ghose et al. 1984a; Ghose et al. 1985; Robie et al. 1988; Ghose et al. 1989; Ghazi-Bayat et al. 1992). In the high temperature orthorhombic phase, iron occupies two distinct octahedral positions: (1) the 8*d* position (labeled M1) and (2) the 4*c* position (labeled M2). The M1 site is randomly occupied by Fe^{2+} and Fe^{3+}, whereas M2 is completely filled by Fe^{2+}. Below the transition temperature, electron ordering between Fe^{2+} and Fe^{3+} cations occurs, causing a small deviation from the orthorhombic *Pnam* symmetry; as the mirror plane normal to the **c** axis is lost, the eightfold M1 site splits into two independent crystallographic sites, M11 (4*e*) and M12 (4*e*), which mainly accommodate Fe^{2+} and Fe^{3+}, respectively.

Several monoclinic structure refinements have been performed using both single crystal X-ray intensities (Finger et al. 1982; Takéuchi et al. 1983; Ghose et al. 1985; Finger and Hazen 1987; Ghose et al. 1989; Takéuchi et al. 1993; Carrozzini 1994; Takéuchi et al. 1994; Bonazzi and Bindi 1999) and powder neutron diffraction data (Ghose et al. 1984b). Structural, thermophysical, magnetic, and electrical properties have been determined over a wide range of *P-T* conditions (Yamanaka and Takéuchi 1979; Nolet and Burns 1979; Evans and Amthauer 1980; Litterst and Amthauer 1984; Finger and Hazen 1987; Ghazi-Bayat et al. 1987; Robie et al. 1988; Ghose 1988; Xuemin et al. 1988; Ghazi-Bayat et al. 1989; Ghazi-Bayat et al. 1992; Ghazi-Bayat et al. 1993; Schmidbauer and Amthauer 1998; Amthauer et al. 1998).

Although not usually considered a rock-forming mineral, ilvaite is often an abundant constituent of Fe and Zn skarns (Burt 1971; Einaudi et al. 1981). It can replace hedenbergite (Logan 2000) and, as a result of an unusual set of conditions, it was found to occur as an alteration product replacing fayalitic olivine in the Skaergaard intrusion (Naslund et al. 1983). Ilvaite probably formed during serpentinization of peridotite (Agata and Adachi 1995), and ilvaite occurring in rodingites associated with serpentinite (Lucchetti 1989) has also been reported. The chemical composition of ilvaite is often close to that of the ideal end-member, with only minor amounts of other cations such as Ti^{4+}, Mg^{2+}, Al^{3+}, and Mn^{2+}. The most common and quantitatively relevant substituent is Mn^{2+}, which mainly replaces Fe^{2+} at the octahedral sites but can also substitute for Ca at the seven-coordinated site (Carrozzini 1994). According to Ghazi-Bayat et al. (1992), Mn content affects the degree of monoclinicity (β angle close to 90.0° when Mn^{2+} = 0.19) and, therefore, the transition temperature, which decreases with increasing Mn^{2+} content (Amthauer et al. 1998). However, as Takéuchi et al. (1983) pointed out, the value of the monoclinic angle is not only related to the degree of disordering. An apparent orthorhombic symmetry, in fact, can be easily simulated by the co-existence of fine components polysynthetically twinned on both (001) and (100); such a twinning would be easily generated if positional mistakes in the cation array take place during the Fe^{2+}-Fe^{3+} ordering process, which occurs when the crystal is cooled through the phase transition temperature (Takéuchi et al. 1994). Takéuchi et al. (1993, 1994) investigated crystals from Kamioka mine, with Mn ranging from 0.19–

* E-mail: pbcry@steno.geo.unifi.it

0.22 apfu (atoms per formula unit; Tochibora skarn) to 0.52 apfu (Maruyama skarn). Taking into account the findings of these authors, who cast doubt on the existence of intrinsically orthorhombic ilvaites in nature, Mn incorporation more likely should induce polysynthetic twinning, rather than cause a monoclinic to orthorhombic phase transition.

A still unresolved problem concerns the ordering of Mn^{2+} among the octahedral sites. Ghazi-Bayat et al. (1989) reported the results of X-ray powder diffraction and Mössbauer studies on synthetic $CaFe^{2+}_{2-x}Mn_xFe^{3+}(Si_2O_7)O(OH)$, with $x = 0.00, 0.12, 0.15, 0.19$, and concluded that Mn^{2+} replaces Fe^{2+} at both the M11 (8*d*) and M2 (4*c*) sites and not preferentially at one site (M2) as previously found by Haga and Takéuchi (1976). According to Cesena et al. (1995), their Mössbauer data obtained for synthetic Mn-bearing ilvaite allowed an unambiguous assignment of Mn^{2+} to the M11 site. By contrast, accurate structural data reported by Carrozzini (1994) showed a good linear relationship between the Mn content and <M2-O>. However, a partially disordered distribution of Mn^{2+} over all the cation sites was proposed by this author for Mn-rich crystals (up to 0.58 apfu) from Oridda (Sardinia, Italy). Ilvaites with higher Mn contents have also been described (Plimer and Ashley 1978; Meinert, 1987; Logan 2000) but no crystallographic data were reported.

The present study was undertaken to provide a crystal-chemical characterization of an ilvaite sample from Perda Niedda mine (Sardinia, Italy) exhibiting an unusually high manganese content (up to 0.73 apfu). In addition, the structural variations induced by heating the sample in air were examined, and compared to those previously reported for heated ilvaite having a chemical composition close to that of the end-member (Bonazzi and Bindi 1999). In accordance with the previous finding, ilvaite easily undergoes the heat-induced ilvaite → oxy-ilvaite transformation, involving both hydrogen loss and iron oxidation. Because of charge balance requirements, oxidation involves only Fe^{2+} located at the M1 site (Bonazzi and Bindi 1999). Keeping this in mind, as well as the crystal chemical differences between Fe^{3+} and Mn^{3+}, it should also be possible to obtain evidence of the manganese ordering, if any, between the M1 and M2 sites.

Experimental methods

Six single crystals of manganoan ilvaite from a skarn at the Perda Niedda mine, Sardinia, Italy (sample no. 10297/509, Mineralogical Museum of the University of Florence) were selected and unit-cell parameters were determined by means of least-squares refinement of the setting angles of 25 reflections ($16 < \vartheta < 25°$) measured with a CAD4 single-crystal diffractometer (Table 1). Subsequently, the same crystals were used for chemical analysis. Chemical compositions were determined using a JEOL JXA 8600 electron microprobe operating at 15 kV and 10 nA and equipped with four wavelength-dispersive spectrometers. Table 2 reports the chemical data and the atomic proportions calculated on the basis of six cations. On the basis of its Mn content, the crystal labeled PN6 was selected for the heat treatments and the structural study. For this purpose, it was subsequently removed from the resin and the unit-cell parameters were determined again. Intensity data were collected in the ϑ-range 2–35°, using graphite-monochromatized Mo$K\alpha$ radiation. Data were subsequently corrected for Lorentz-polarization and absorption effects (North et al. 1968). The crystal was annealed in air for 48 h at selected temperatures ranging from 400 to 700 °C using a magnetic release furnace that allows rapid cooling to room temperature. After each heat treatment, determination of unit-cell parameters and intensity data collection was repeated (experimental conditions are given in Table 3). As the annealing temperature increased, reflections became broader and weaker; after the annealing at 700 °C, the intensities were no longer collected.

Table 1. Unit-cell parameters for selected crystals of ilvaite from Perda Niedda

	a (Å)	*b* (Å)	*c* (Å)	β (°)	*V* (Å³)
PN1-*RT*	12.988(7)	8.829(2)	5.844(3)	90.19(3)	670.1(6)
PN2-*RT*	13.000(8)	8.835(5)	5.837(8)	90.05(7)	670.4(7)
PN3-*RT*	12.995(3)	8.839(2)	5.840(1)	90.15(2)	670.8(4)
PN4-*RT*	13.008(5)	8.844(1)	5.847(2)	90.20(2)	672.7(4)
PN5-*RT*	13.017(6)	8.857(1)	5.846(2)	90.26(2)	674.0(5)
PN6-*RT*	13.014(5)	8.867(3)	5.838(4)	90.02(4)	673.7(5)
PN6-400	13.015(6)	8.868(1)	5.842(2)	90.01(2)	674.3(5)
PN6-500	13.008(7)	8.865(2)	5.845(3)	90.00(2)	674.0(6)
PN6-600	12.993(7)	8.864(2)	5.837(2)	90.00(2)	672.2(6)
PN6-650	12.983(8)	8.868(3)	5.822(2)	90.00(2)	670.3(6)
PN6-675	12.992(6)	8.869(2)	5.820(1)	90.00(2)	670.6(5)
PN6-690	13.015(6)	8.873(2)	5.816(1)	90.00(2)	671.6(5)
PN6-700	13.032(5)	8.877(2)	5.812(1)	90.00(2)	672.4(6)

Table 2. Chemical composition (wt%) and atomic proportions of the crystals from Perda Niedda

	PN1-*RT*	PN2-*RT*	PN3-*RT*	PN4-*RT*	PN5-*RT*	PN6-*RT*
SiO_2	29.22	29.37	29.11	29.27	29.06	29.31
TiO_2	–	0.09	0.12	–	–	–
Fe_2O_3	19.66	19.36	19.46	19.59	20.03	19.56
Al_2O_3	–	0.08	0.26	0.26	0.02	–
FeO	27.13	26.21	26.06	25.73	24.13	22.49
CaO	12.18	13.17	13.10	13.33	13.27	13.47
MnO	9.61	9.52	9.33	9.43	11.00	12.86
MgO	0.07	0.06	0.08	0.12	0.06	0.03
Total	97.87	97.86	97.52	97.73	97.57	97.72
Si^{4+}	1.993	1.997	1.985	1.989	1.983	1.994
Ti^{4+}	–	0.004	0.006	–	–	–
Fe^{3+}	1.009	0.990	0.998	1.002	1.028	1.001
Al^{3+}	–	0.006	0.021	0.020	0.002	–
Fe^{2+}	1.547	1.490	1.486	1.463	1.377	1.279
Ca^{2+}	0.890	0.959	0.957	0.971	0.970	0.982
Mn^{2+}	0.555	0.548	0.539	0.543	0.635	0.741
Mg^{2+}	0.006	0.006	0.008	0.012	0.005	0.003
Σ cations	6.000	6.000	6.000	6.000	6.000	6.000

Notes: Partition between FeO and Fe_2O_3 was calculated in order to ensure charge neutrality. H_2O was not determined.

As shown in Table 3, the β angle value for the untreated PN6 crystal was found to be 90.00° within the limits of experimental error. Only five 0*kl* reflections with $k + l = 2n + 1$ were observed (i.e., 041, 061, 032, 052, 054), showing $[F_o/\sigma(F_o)] \leq 5.0$. After heating at 400 °C, no systematic absence violations were found.

Structure refinements were performed using the SHELXL-93 program (Sheldrick 1993), with weighting scheme $w = k/\sigma^2_{Fo}$. Scattering factors and correction factors were taken from the *International Tables for X-ray Crystallography*, vol. IV (Ibers and Hamilton 1974). As for PN6-*RT*, least squares were run in both monoclinic ($R_{obs} = 2.79\%$) and orthorhombic symmetry ($R_{obs} = 2.59\%$). The atomic arrangement obtained by re-

TABLE 3. Experimental details of intensity data collections and structure refinements

	PN6-*RT*	PN6-400	PN6-500	PN6-600	PN6-650	PN6-675	PN6-690
space group	*Pnam*	*Pnam*	*Pnam*	*Pnam*	*Pnam*	*Pnam*	*Pnam*
scan mode	ω	ω	ω	ω	ω	ω	ω
scan width (°/min)	2.2	2.2	2.2	2.2	2.5	2.5	2.5
scan speed (°/min)	4.12	4.12	4.12	4.12	2.75	2.75	2.06
no.coll.refl.	6390	6392	6401	6372	3346	3333	3346
no.ind.refl.	1598	1600	1601	1594	1590	1587	1593
no.obs.refl.	1542	1442	1476	1492	1483	1321	1307
no.ref.par.	88	88	88	88	88	85	85
R_{symm}(%)	4.25	3.23	2.91	3.79	2.45	3.28	3.31
R_{obs} (%)	2.59	2.04	2.70	4.55	3.28	2.86	4.32
R_{all} (%)	2.71	2.53	3.07	4.83	3.66	3.99	5.65
R^*_{all} (%)	2.56	2.40	2.93	4.62	3.48	3.83	5.49

Note: R^*_{all} is calculated for merged reflections.

finement in the monoclinic space group ($P2_1/a$) clearly showed orthorhombic symmetry, with Fe^{2+} and Fe^{3+} completely disordered between two independent 4*e* positions (M11 and M12); subsequent structure refinements were performed in space group *Pnam*. Keeping in mind that the apparent orthorhombic symmetry, as discussed above, can be reasonably related to the presence of twinned ordered domains, in the following discussion we will refer to the orthorhombic structure. Details of refinements are given in Table 3. Fractional coordinates and isotropic equivalent displacement parameters are given in Table 4.

RESULTS AND DISCUSSION

Description of the structure

The atomic arrangement of ilvaite is formed of octahedral ribbons linked by Si_2O_7 groups and Ca polyhedra. Hydrogen bonds, directed approximately along the a axis, also connect neighboring ribbons. These ribbons run parallel to the c axis and consist of edge-sharing double chains of M1 octahedra, with the larger M2 octahedra alternatively attached above and below by means of four shared edges. Bond distances and distortion parameters are given in Table 5.

Effects of the $Mn^{2+} \leftrightarrow Fe^{2+}$ substitution

Before heating, the PN6 crystal shows a structural arrangement quite similar to that of ilvaites exhibiting a very low monoclinicity (Beran and Bittner 1974; Takéuchi et al. 1994). The value of the <Ca-O> distance (2.410 Å) and the refined site-scattering of the A site (close to 20.0 electrons) suggest that, in spite of the high Mn content, no extensive $Ca \leftrightarrow Mn^{2+}$ substitution occurs. The value of the <M1-O> distance (2.081 Å) is quite similar to that observed for the grand mean <M11, 12–O> in Mn-poor ilvaites (i.e., 2.078–2.081 Å, according to Beran and Bittner 1974; Finger and Hazen 1987; Carrozzini 1994; Bonazzi and Bindi 1999), thus suggesting that no remarkable Mn^{2+} substitution occurs at the M1 site. On the contrary, the value of the <M2-O> distance (2.207 Å) is unusually high when compared to the corresponding value for Mn-free ilvaites (2.187–2.188 Å for crystals from Seriphos having Mn = 0.02 apfu; Finger and Hazen 1987; Carrozzini 1994). The <M2-O> observed in PN6-*RT* appears even higher than those found in Mn-rich ilvaites from Oridda (<M2-O> = 2.199–2.201, Mn_{M2} = 0.36–0.42 apfu; Carrozzini 1994) and Maruyama (<M2-O> = 2.201 Å Mn_{M2} = 0.50 apfu; Takéuchi et al. 1993). According to the model proposed by Carrozzini (1994), the <M2-O> distance (2.207 Å) observed here would be consistent with an Mn^{2+} replacing Fe^{2+} content of 0.59 apfu, a value much lower than that predicted on the basis of the analytical data ($Mn_{M2} \sim 0.74_{tot} - 0.02_A - 0.00_{M1} \sim 0.72$ apfu). The model proposed appears in fact to underestimate the amount of manganese entering the M2 site, especially in the case of ilvaites with extremely high Mn contents, such as the Maruyama crystal (0.41 instead of 0.50 as proposed by Takéuchi et al. 1994). On the basis of the fact that <M1-O>, independently of the total Mn content, is quite invariable in most of the ilvaite structures previously published, we can assume that only negligible amounts of Mn^{2+} replace Fe^{2+} at M1. Therefore, the structural data available in the literature (references in Fig. 1) were used to calculate a new regression line assuming $Mn_{M2} = Mn_{oct} = Mn_{tot} - Mn_A$. As discussed below, the crystals from the Tochibora skarn (Takéuchi et al. 1993) likely exhibit a more disordered Mn distribution, so they were not included in the model. The following linear equation was obtained: <M2-O> = 2.1869(3) + 0.0266(9) Mn^{2+} (apfu) (r = 0.992). The intercept (<Fe^{2+}-O> = 2.187 Å) is identical to the value resulting from the model proposed by Carrozzini (1994), whereas the theoretical value for <Mn^{2+}-O> differs slightly in the two models (2.214 instead of 2.221 Å). It is worth noting that the grand mean <M11, 12-O> distances (2.080 Å for all the crystals) for the ilvaite material from Oridda, for which a disordered model had been proposed (Carrozzini 1994), agrees perfectly with the values found for M1 sites randomly occupied by Fe^{2+} and Fe^{3+} alone. On the contrary, the crystals from Tochibora skarn examined by Takéuchi et al. (1993) exhibit slightly greater values for <M11, 12-O>. According to the new model, the predicted Mn_{M2} content for the ilvaites from Oridda (0.45, 0.53, and 0.53 for the three crystals studied, respectively) is consistent with an intermediate solid solution between ilvaite and a hypothetical $CaFe^{2+}Mn^{2+}Fe^{3+}(Si_2O_7)O(OH)$ end-member. In the sample from Perda Niedda, solid solution extends toward a higher manganoan component (up to 70%).

As previously reported by Carrozzini (1994), a linear relationship can be observed between the Mn content and the *b* parameter, while *a* and *c* are not as markedly affected by the incorporation of this element (Fig. 2). The reason is that the replacement of Fe^{2+} by Mn^{2+} in the distorted (2 + 4) M2-octahedron causes a significant lengthening of the shortest M2-O1 and M2-O6 distances, which are both directed along the **b** axis. By plotting *b* against the octahedral Mn content a linear trend was obtained for data reported here and from the literature, with the exception of the synthetic crystals examined by Ghazi-Bayat et al. (1989) and the crystals from Tochibora skarn studied by Takéuchi et al. (1993). For the synthetic crystals, a possible reason for this feature could be the disordered distribution of Mn between M11 and M2 inferred on the basis of Mössbauer experiments (Ghazi-Bayat et al. 1989). A minor Mn disordering could be hypothesized for the Tochibora crystals as well. The resulting regression line, b = 8.799(2) + 0.081(5) Mn^{2+}(apfu) (r = 0.967), agrees fairly well with the model [b = 8.799(3) + 0.092(6) Mn^{2+}(apfu)] previously proposed by Carrozzini (1994).

TABLE 4. Fractional atomic coordinates and isotropic displacement parameters, with e.s.d. values in parentheses

		PN6-*RT*	PN6-*400*	PN6-5*00*	PN6-*600*	PN6-*650*	PN6-*675*	PN6-*690*
A	*x*	0.81315(3)	0.81319(3)	0.81372(4)	0.81602(8)	0.81841(5)	0.81901(5)	0.81955(8)
	y	0.37051(5)	0.37053(4)	0.37114(6)	0.37350(9)	0.37552(7)	0.37614(7)	0.37599(9)
	z	0.75	0.75	0.75	0.75	0.75	0.75	0.75
	U_{eq}	0.0087(1)	0.0084(1)	0.0089(1)	0.0102(2)	0.0108(1)	0.0114(1)	0.0132(2)
M1	*x*	0.89039(2)	0.89034(1)	0.89014(2)	0.88944(4)	0.88865(3)	0.88846(2)	0.88830(4)
	y	0.05037(2)	0.05046(2)	0.05101(3)	0.05336(6)	0.05553(4)	0.05634(3)	0.05682(5)
	z	0.00620(4)	0.00585(3)	0.00451(5)	–0.00094(9)	–0.00472(6)	–0.00567(5)	–0.00600(9)
	U_{eq}	0.0072(1)	0.0071(1)	0.0074(1)	0.0086(16)	0.0081(1)	0.0081(1)	0.0094(2)
M2	*x*	0.93911(2)	0.93914(2)	0.93837(3)	0.93451(7)	0.93070(4)	0.92967(4)	0.92869(6)
	y	0.73858(3)	0.73861(3)	0.73842(5)	0.73764(9)	0.73692(6)	0.73665(5)	0.73676(8)
	z	0.25	0.25	0.25	0.25	0.25	0.25	0.25
	U_{eq}	0.0075(1)	0.0072(1)	0.0077(1)	0.0092(2)	0.0094(1)	0.0097(1)	0.01110(2)
Si1	*x*	0.95892(4)	0.95900(4)	0.95958(5)	0.9623(1)	0.9647(1)	0.9654(1)	0.9666(1)
	y	0.36652(6)	0.36670(6)	0.36646(8)	0.3655(2)	0.3644(1)	0.3644(1)	0.3638(1)
	z	0.25	0.25	0.25	0.25	0.25	0.25	0.25
	U_{eq}	0.0060(1)	0.0057(1)	0.0060(1)	0.0069(3)	0.0075(2)	0.0080(2)	0.0095(3)
Si2	*x*	0.67992(4)	0.67995(4)	0.68051(5)	0.6829(1)	0.6853(1)	0.6861(1)	0.6869(1)
	y	0.22666(6)	0.22664(6)	0.22740(8)	0.2303(2)	0.2333(1)	0.2343(1)	0.2349(1)
	z	0.25	0.25	0.25	0.25	0.25	0.25	0.25
	U_{eq}	0.0060(1)	0.0059(1)	0.0062(1)	0.0071(3)	0.0066(2)	0.0065(1)	0.0073(2)
O1	*x*	0.0093(1)	0.0096(1)	0.0100(2)	0.0132(3)	0.0149(2)	0.0154(2)	0.0162(3)
	y	0.0250(2)	0.0257(2)	0.0252(2)	0.0229(5)	0.0214(3)	0.0212(2)	0.0198(4)
	z	0.75	0.75	0.75	0.75	0.75	0.75	0.75
	U_{eq}	0.0124(3)	0.0123(3)	0.01231(4)	0.0127(7)	0.0112(4)	0.0114(4)	0.0137(7)
O2	*x*	0.9367(1)	0.9367(1)	0.9372(1)	0.9393(2)	0.9423(1)	0.9430(1)	0.9439(2)
	y	0.2712(1)	0.2714(1)	0.2711(2)	0.2699(3)	0.2690(2)	0.2687(2)	0.2683(3)
	z	0.0152(2)	0.0155(2)	0.0155(2)	0.0151(5)	0.0147(3)	0.0147(2)	0.0143(4)
	U_{eq}	0.0086(2)	0.0085(2)	0.0088(2)	0.0105(5)	0.0103(3)	0.0109(3)	0.0125(4)
O3	*x*	0.7771(1)	0.7771(1)	0.7776(1)	0.7809(3)	0.7832(2)	0.7838(2)	0.7850(3)
	y	0.1081(2)	0.1080(2)	0.1089(2)	0.1111(4)	0.1139(2)	0.1148(2)	0.1144(4)
	z	0.25	0.25	0.25	0.25	0.25	0.25	0.25
	U_{eq}	0.0088(3)	0.0086(2)	0.0085(3)	0.0085(6)	0.0092(4)	0.0095(4)	0.0120(6)
O4	*x*	0.6716(1)	0.6716(1)	0.6720(1)	0.6734(2)	0.6757(1)	0.6761(1)	0.6761(2)
	y	0.3292(1)	0.3292(1)	0.3299(2)	0.3326(3)	0.3351(2)	0.3359(2)	0.3358(3)
	z	0.0183(2)	0.0186(2)	0.0184(2)	0.0184(5)	0.0168(3)	0.0164(2)	0.0159(4)
	U_{eq}	0.0086(2)	0.0082(2)	0.0083(2)	0.0094(5)	0.0101(3)	0.0103(3)	0.0135(4)
O5	*x*	0.5844(1)	0.5846(1)	0.5850(1)	0.5880(3)	0.5908(2)	0.5917(2)	0.5922(3)
	y	0.1025(2)	0.1022(2)	0.1031(2)	0.1054(5)	0.1083(3)	0.1089(2)	0.1091(4)
	z	0.25	0.25	0.25	0.25	0.25	0.25	0.25
	U_{eq}	0.0085(3)	0.0081(2)	0.0082(3)	0.0111(6)	0.0109(4)	0.0107(4)	0.0128(6)
O6	*x*	0.6039(1)	0.6036(1)	0.6028(2)	0.5995(4)	0.5959(2)	0.5951(2)	0.5928(4)
	y	0.0207(2)	0.0211(2)	0.0208(2)	0.0195(5)	0.0184(3)	0.0183(3)	0.0181(4)
	z	0.75	0.75	0.75	0.75	0.75	0.75	0.75
	U_{eq}	0.0121(3)	0.0121(3)	0.0128(4)	0.0172(8)	0.0173(5)	0.0182(5)	0.0219(8)
O7	*x*	0.7978(1)	0.7978(1)	0.7983(2)	0.8026(4)	0.8067(2)	0.8074(2)	0.8095(3)
	y	0.1100(2)	0.1101(2)	0.1113(2)	0.1140(5)	0.1147(3)	0.1149(2)	0.1151(4)
	z	0.75	0.75	0.75	0.75	0.75	0.75	0.75
	U_{eq}	0.0087(2)	0.0085(2)	0.0094(3)	0.0121(7)	0.0113(4)	0.0110(4)	0.0114(6)
H	*x*	0.737(3)	0.740(2)	0.746(5)	0.788(13)			
	y	0.068(5)	0.071(4)	0.070(7)	0.058(16)			
	z	0.75000	0.75	0.75	0.75			
	U_{iso}	0.026(9)	0.018(8)	0.05(2)	0.07(5)			

TABLE 5. Structure parameters for PN6 crystal

	PN6-*RT*	PN6-400	PN6-500	PN6-600	PN6-650	PN6-675	PN6-690
A-O2(×2)	2.400(1)	2.401(1)	2.403(1)	2.409(3)	2.420(2)	2.424(2)	2.428(3)
A-O3	2.412(2)	2.412(1)	2.419(2)	2.454(4)	2.492(3)	2.503(2)	2.515(4)
A-O4(×2)	2.446(1)	2.448(1)	2.448(1)	2.454(3)	2.444(2)	2.445(2)	2.450(3)
A-O5	2.451(2)	2.448(1)	2.442(2)	2.404(4)	2.377(3)	2.368(2)	2.366(4)
A-O7	2.319(2)	2.318(1)	2.312(2)	2.307(5)	2.318(3)	2.322(2)	2.319(4)
mean	2.410	2.411	2.411	2.413	2.416	2.419	2.422
M1-O1	2.044(1)	2.046(1)	2.050(2)	2.050(3)	2.057(2)	2.061(2)	2.055(3)
M1-O1'	2.164(1)	2.166(1)	2.167(2)	2.185(3)	2.195(2)	2.200(2)	2.212(3)
M1-O2	2.049(1)	2.051(1)	2.046(1)	2.028(3)	2.020(2)	2.016(2)	2.015(2)
M1-O3	2.112(1)	2.114(1)	2.113(1)	2.097(3)	2.084(2)	2.081(2)	2.070(3)
M1-O4	2.125(1)	2.126(1)	2.124(1)	2.123(3)	2.127(2)	2.128(1)	2.133(2)
M1-O7	1.992(1)	1.991(1)	1.981(1)	1.917(3)	1.856(2)	1.844(1)	1.826(2)
mean	2.081	2.082	2.080	2.067	2.057	2.055	2.052
λ	1.0056	1.0057	1.0056	1.0064	1.0083	1.0089	1.0098
σ^2	15.05	15.39	14.53	13.31	15.26	15.92	16.83
x (Fe^{3+})*	0.50	0.50	0.50	0.62	0.71	0.73	0.75
M2-O1	2.201(2)	2.194(1)	2.201(2)	2.229(4)	2.257(3)	2.263(2)	2.276(4)
M2-O2(×2)	2.240(1)	2.242(1)	2.244(1)	2.255(3)	2.258(2)	2.261(2)	2.262(3)
M2-O4(×2)	2.275(1)	2.277(1)	2.276(1)	2.265(3)	2.254(2)	2.251(2)	2.241(3)
M2-O6	2.011(2)	2.007(2)	2.002(2)	1.983(5)	1.968(3)	1.963(2)	1.960(4)
mean	2.207	2.207	2.207	2.209	2.208	2.208	2.207
λ	1.0213	1.0213	1.0221	1.0262	1.0310	1.0327	1.0341
σ^2	66.13	65.46	67.98	81.95	98.75	104.60	109.73
Si1-O2(×2)	1.636(1)	1.636(1)	1.636(1)	1.639(3)	1.636(2)	1.637(2)	1.638(3)
Si1-O5	1.656(2)	1.658(2)	1.654(2)	1.653(4)	1.655(3)	1.658(2)	1.652(4)
Si1-O6	1.593(2)	1.593(2)	1.591(2)	1.584(5)	1.576(3)	1.575(2)	1.572(4)
mean	1.630	1.631	1.629	1.629	1.626	1.627	1.625
λ	1.0033	1.0032	1.0033	1.0032	1.0040	1.0040	1.0038
σ^2	12.77	12.43	12.74	12.22	15.17	15.38	14.22
Si2-O3	1.645(2)	1.645(1)	1.643(2)	1.655(4)	1.654(3)	1.654(2)	1.665(4)
Si2-O4(×2)	1.633(1)	1.633(1)	1.634(1)	1.632(3)	1.635(2)	1.636(1)	1.636(3)
Si2-O5	1.661(2)	1.661(1)	1.661(2)	1.657(5)	1.653(3)	1.656(2)	1.663(4)
mean	1.643	1.643	1.643	1.644	1.645	1.645	1.650
λ	1.0085	1.0087	1.0087	1.0094	1.0100	1.0104	1.0109
σ^2	32.64	33.32	33.20	35.80	37.49	39.01	40.69
O7-O6	2.645(2)	2.648(2)	2.667(3)	2.769(3)	2.867(3)	2.888(3)	2.949(3)

Note: Distances are reported in angstroms; the mean quadratic elongation (λ) and the angle variance (σ^2) were computed according to Robinson et al. (1971).

* The cation population at M1 was estimated taking into account the values published by Ghose (1969), <Fe^{2+}-O> = 2.135 Å, <Fe^{3+}-O> = 2.025 Å.

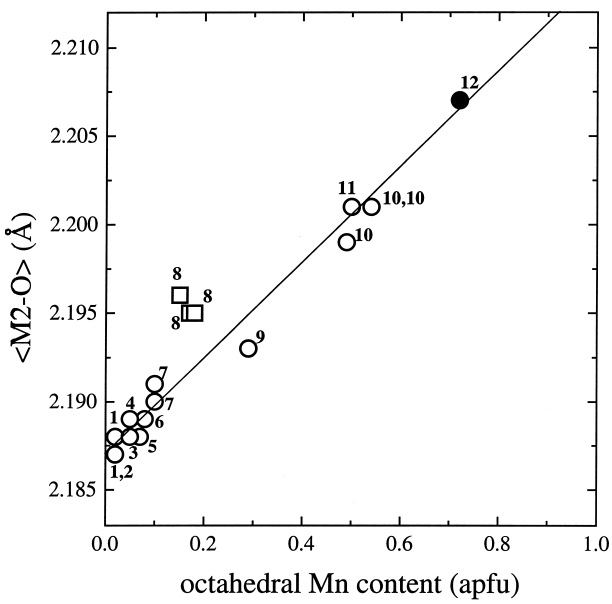

FIGURE 1. Values of the <M2-O> distance plotted against the octahedral Mn content (apfu). Solid symbol (12) refers to the crystal of manganoan ilvaite from Perda Niedda. Open symbols (1–11) refer to data from literature as following: (1) ilvaite from Seriphos, Greece (Carrozzini 1994); (2) ilvaite from Seriphos, Greece (Finger and Hazen 1987); (3) ilvaite from Tsumo, Japan (Takéuchi et al. 1983); (4) ilvaite from Rio Marina, Elba, Italy (Bonazzi and Bindi 1999); (5) ilvaite from Elba, Italy (Finger and Hazen 1987); (6) ilvaite from Rio Marina, Elba, Italy (Carrozzini 1994); (7) ilvaite from Cinco Villas, Spain (Carrozzini 1994); (8) ilvaite from Tochibora, Japan (Takéuchi et al. 1993); (9) ilvaite from Techukhe, Japan (Takéuchi et al. 1983); (10) manganoan ilvaite from Oridda, Sardinia, Italy (Carrozzini 1994); (11) manganoan ilvaite from Marujama, Japan (Takéuchi et al. 1993). Data fit the following equation: <M2-O> = 2.1869(3) + 0.0266(9) Mn^{2+} (apfu), (r = 0.992); crystals from Tochibora skarn (8) were not included in the regression (see text).

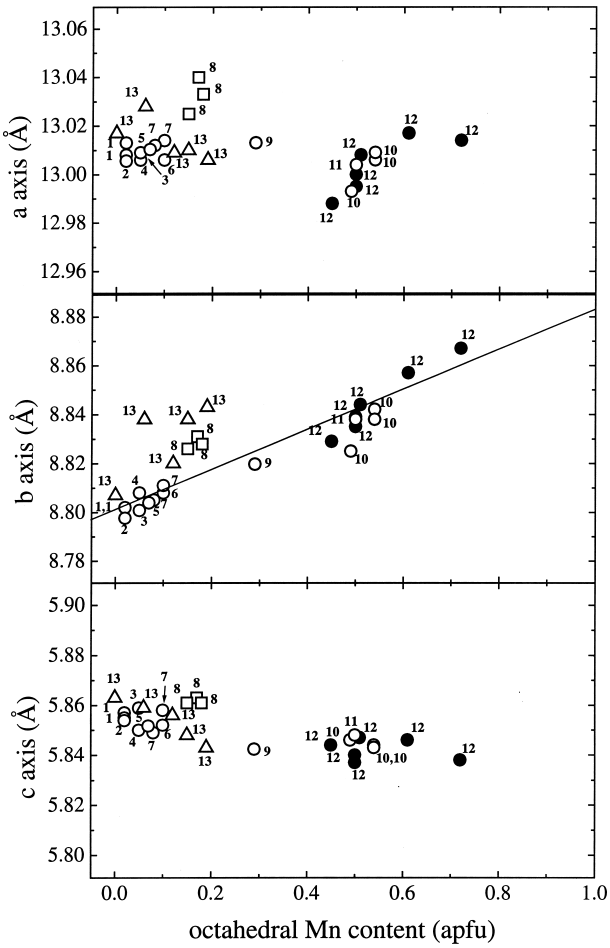

FIGURE 2. Unit-cell parameters plotted against the octahedral Mn content (apfu). Solid symbols (12) refer to the crystals of manganoan ilvaite from Perda Niedda. Open symbols refer to data from literature as following: (1–11) as in Figure 1; (13) synthetic Mn-bearing ilvaite (Ghazi-Bayat et al. 1989).

Effects of heat treatments

As previously observed for the Mn-poor ilvaite from Rio Marina, Elba (Bonazzi and Bindi 1999), the M2 octahedron, Ca–polyhedron, and both Si tetrahedra do not show marked variations in their average bond distances with increasing temperature. Minor adjustments in individual bond distances and angles are due to the marked variations involving the M1 site and the hydrogen bonding system, which, however, occur without any change in space group symmetry or topology. No appreciable changes are observed up to 500 °C. Following heating at 600 °C, iron oxidation is evident from the decreasing <M1-O> distance [from 2.080 Å (PN6-*500*) down to 2.052 Å (PN6-690) (Table 5)]. Taking into account the values published by Ghose (1969), the M1 site population was estimated for each step (see Table 5), with the assumption that no cation disordering occurs between the M1 and M2 sites during the oxidation-dehydrogenation process. This hypothesis appears to be reasonable, as the <M2-O> distance is invariable over the whole temperature range. With the increase of the $[Fe^{3+}/(Fe^{2+} + Fe^{3+})]_{M1}$ ratio and the consequent decrease of the volume of the M1 octahedron, the large and distorted M2 octahedron, sharing four edges with four M1 octahedra, becomes even more irregular (σ^2_{M2} ranging from 66.13 for PN6-*RT* to 109.73 for PN6-690; λ_{M2} ranging from 1.0213 for PN6-*RT* to 1.0341 for PN6-690). As a consequence of a greater electrostatic cation repulsion between M2 and M1 cations occurring with increasing $[Fe^{3+}/(Fe^{2+} + Fe^{3+})]_{M1}$, the M2 cation moves toward the apical O6 oxygen atom (Fig. 3) and the M2-M1 distances increase accordingly.

The most pronounced evidence of hydrogen loss accompanying the oxidation reaction is the lengthening of the donor (O7)-acceptor (O6) distance (Fig. 4), which increases markedly after annealing at 600 °C (from 2.667 Å in PN6-500 to 2.949 Å in PN6-690). The loss of positive charge to the O7-O atom due to partial dehydrogenation is directly compensated by the oxidation of divalent iron at M1, as shown from the trend of the M1-O7 distance, which decreases with the ongoing oxidation-dehydrogenation process (Fig. 3). On the other hand, the A-O7 bond distance, the shortest within the A polyhedron, does not change significantly with heating. The loss of positive charge to the acceptor O atom (O6) is balanced by shortening of the M2-O6 distance, and, to a lesser extent, of the Si1-O6 distance. Table 6 reports the results of the electrostatic charge balance computed (without the hydrogen contribution) according to Brown and Altermatt (1985). At the beginning of the heating process, the resulting empirical bond-valence sums for O7 and O6 are 1.41 and 1.65 valence units, respectively, as expected for an O7-H···O6 hydrogen-bond system. As the heating temperature increases, hydrogen is partially lost, and the total bond valence for O7 and O6 increases

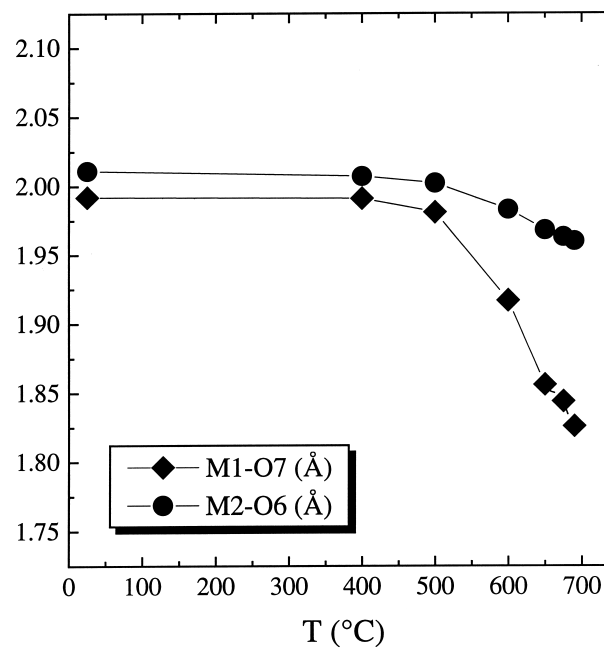

FIGURE 3. M1-O7 and M2-O6 distances plotted against the heating temperature.

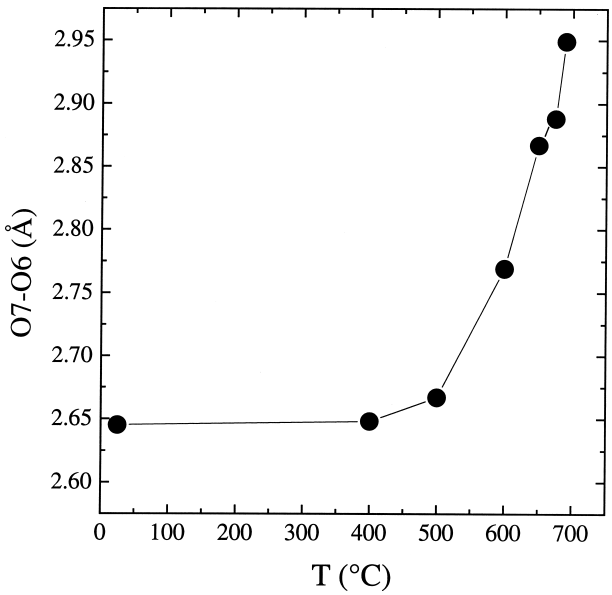

FIGURE 4. The donor-acceptor distance (O7-O6) plotted against the heating temperature.

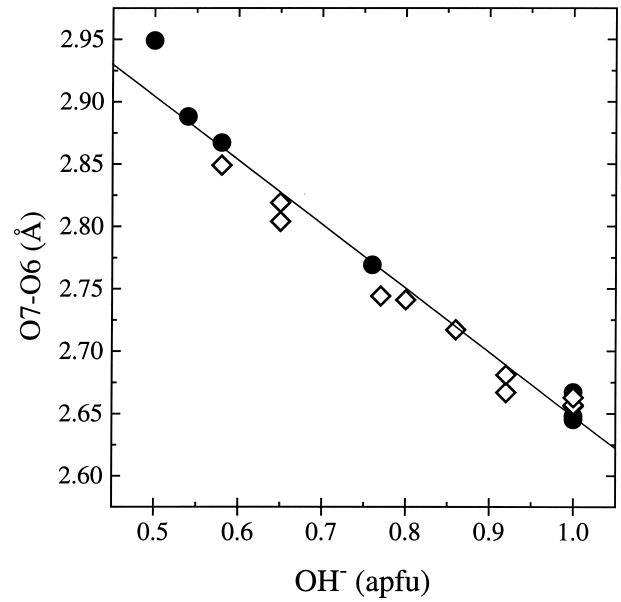

FIGURE 5. Relationship between the donor-acceptor distance and the OH^- content in heated ilvaites. Squares refer to ilvaite from Elba, Italy (Bonazzi and Bindi 1999); circles refer to PN6 crystal (this study).

TABLE 6. Empirical bond-valence sums for the oxygen atoms of the manganoan ilvaite structure heated at increasing temperatures

	PN6-*RT*	PN6-400	PN6-500	PN6-600	PN6-650	PN6-675	PN6-690
O1	1.90	1.90	1.87	1.81	1.74	1.71	1.68
O2	2.02	2.02	2.01	2.01	2.00	2.00	1.99
O3	2.04	2.03	2.03	2.01	2.01	2.01	2.01
O4	1.92	1.92	1.91	1.92	1.93	1.93	1.94
O5	2.14	2.14	2.15	2.19	2.21	2.21	2.22
O6	1.65	1.66	1.67	1.71	1.75	1.76	1.77
O7	1.41	1.41	1.44	1.65	1.86	1.90	1.97

Note: Bond valences are weighted assuming A = 0.98 Ca + 0.02 Mn^{2+}; M1 = x Fe^{3+} + (1–x) Fe^{2+} (x as in Table 5); M2 = 0.72 Mn^{2+} + 0.28 Fe^{2+}. The empirical parameters used in the calculations are those of Brown and Altermatt (1985).

accordingly. However, during the process, the bond valence sum for the O7 oxygen atom increases much more quickly than that for O6, and, after heating at 650 °C, the sum for O7 becomes greater than the sum for O6. Such an unexpected behavior could be due to migration of the remaining hydrogen atom from O7 toward O6. Unfortunately, a reliable location of the hydrogen atom on the ΔF-Fourier map was not possible for PN6-650.

In order to establish a relationship between the donor-acceptor distance and the OH^- content, we can tentatively assume, for each step of the heat-treatment process, a content of hydrogen such that charge neutrality of the chemical formula is achieved (Fe^{3+} content estimated on the basis of <M1-O>). In Figure 5 the O7-O6 distance is plotted against the OH^- content (atoms per formula unit), combining the PN6 crystal data together with those obtained for the Mn-poor ilvaite previously studied (Bonazzi and Bindi 1999). The corresponding regression line is O7-O6 = 3.16(2) – 0.51(2)[OH^-] (apfu) (r = –0.985). The O7-O6 value found for PN6-690 (2.949 Å), higher than that predicted on the basis of the obtained model (2.91 Å), suggests a degree of oxidation-dehydrogenation even greater than that (about 50%) estimated on the basis of the <M1-O> distance. The results of the charge balance for the final step of the heat treatment are in keeping with this hypothesis.

This structural investigation on a natural ilvaite sample exhibiting the highest Mn content known provides unambiguous evidence that Mn^{2+} substitutes for Fe^{2+} dominantly in the M2 site. This conclusion is in keeping with the results from natural Mn-bearing ilvaites previously studied (Haga and Takéuchi 1976; Carrozzini 1994), while it is apparently in contrast with the results from synthetic Mn-bearing ilvaites (Ghazi-Bayat et al. 1989; Cesena et al. 1995) that, however, exhibit rather low Mn doping. Additional work will be necessary to clarify whether the different behavior between synthetic and natural crystals may be due to the experimental conditions of synthesis and/or the different concentrations of Mn. Finally, the effects of such a high content of Mn in the sample from Perda Niedda mine on the thermophysical, magnetic, and electric properties of ilvaite are worth of further investigations.

ACKNOWLEDGMENTS

Critical and careful reviews by F. J. Litterst and an anonymous reviewer were greatly appreciated. The authors thank F. Olmi (C.N.R. Centro di Studi per la Minerogenesi e la Geochimica Applicata, Firenze) for his contribution to chemical analyses. This work was funded by C.N.R. and by M.U.R.S.T. (cofinanziamento 1999, project "Transformations, reactions, ordering in minerals").

REFERENCES CITED

Agata, T. and Adachi, M. (1995) Ilvaite from a serpentinized peridotite in the Asama igneous complex, Mikabu greenstone belt, Sambagawa metamorphic terrain, central Japan. Mineralogical Magazine, 59, 489–496.

Amthauer, G., Lottermoser, W., Redhammer, G., and Tippelt, G. (1998) Mössbauer studies of selected synthetic silicates. Hyperfine Interactions, 113, 219–248.

Bartholomé, P., Duchesne, J.C., and Van der Plas, L. (1968) Sur une forme monoclinique de l' ilvaite. Annales de la Société Geologique de Belgique, 90, 779–788.

Belov, N.V. and Mokeeva, V.I. (1954) The crystal structure of ilvaite (in Russian). Trudy Instituta Kristallografiya Akademiya Nauk. SSSR, 9, 89–102.

Beran, A. and Bittner, H. (1974) Untersuchungen zur Kristallchemie des Ilvaits. Tschermaks Mineralogische und Petrologische Mitteilungen, 21, 11–29.

Bonazzi, P. and Bindi, L. (1999) Structural adjustments induced by heat treatment in ilvaite. American Mineralogist, 84, 1604–1612.

Brown, I.D. and Altermatt, D. (1985) Bond-valence parameters obtained from a systematic analysis of the inorganic crystal structure database. Acta Crystallographica, B41, 244–247.

Burt, D.M. (1971) The facies of some Ca-Fe-Si skarns in Japan. Carnegie Institute Washington Yearbook, 70, 185–188.

Carrozzini, B. (1994) Crystal structure refinements of ilvaite: new relationships between chemical composition and crystallographic parameters. European Journal of Mineralogy, 6, 465–479.

Cesena, M., Schepke, M., De Melo, M.A.C., Litterst, F.J., and Amthauer, G. (1995) Mössbauer studies of Mn- and Al- doped synthetic ilvaites. Journal of Magnetism and Magnetic Materials, 140–144, 1889–1890.

Einaudi, M.T., Meinert, L.D., and Newberry, R.J. (1981) Skarn deposits. Economic Geologic 75th Anniversary volume, 317–391.

Evans, B.J. and Amthauer, G. (1980) The electronic structure of ilvaite and the pressure and temperature dependence of its ^{57}Fe Mössbauer spectrum. Journal of Physics and Chemistry of Solids, 41, 985–1001.

Finger, L.W. and Hazen, R.M. (1987) Crystal structure of monoclinic ilvaite and the nature of the monoclinic-orthorhombic transition at high pressure. Zeitschrift für Kristallographie, 179, 415–430.

Finger, L.W., Hazen, R.M., and Hughes, J.M. (1982) Crystal structure of monoclinic ilvaite. Carnegie Inst. Washington Yearbook, 81, 386–388.

Ghazi-Bayat, B., Amthauer, G., Schürmann, K., and Hellner, E. (1987) Synthesis and characterization of the mixed valent iron silicate ilvaite, $CaFe_3[Si_2O_7/O/(OH)]$. Mineralogy and Petrology, 37, 97–108.

Ghazi-Bayat, B., Amthauer, G., and Hellner, E. (1989) Synthesis and characterization of Mn-bearing ilvaite $CaFe^{2+}_{2-x}Mn_xFe^{3+}[Si_2O_7/O/(OH)]$. Mineralogy and Petrology, 40, 101–109.

Ghazi-Bayat, B., Behruzi, M., Litterst, F.J., Lottermoser, W., and Amthauer, G. (1992) Crystallographic phase transition and valence fluctuation in synthetic Mn-bearing ilvaite $CaFe^{2+}_{2-x}Mn^{2+}_xFe^{3+}[Si_2O_7/O/(OH)]$. Physics and Chemistry of Minerals, 18, 491–496.

Ghazi-Bayat, B., Amthauer, G., and Ahsbahs, H. (1993) High pressure X-ray diffraction study of ilvaite $CaFe^{2+}_2Fe^{3+}[Si_2O_7/O/(OH)]$. Physics and Chemistry of Minerals, 20, 402–406.

Ghose, S. (1969) Crystal chemistry of iron. In K.H. Wedelpohl, Ed., Handbook of Geochemistry, II-3, 26A–10. Springer-Verlag, Berlin.

———(1988) Charge localization and associated crystallographic and magnetic phase transitions in ilvaite, a mixed-valence iron silicate. In S. Ghose, J.M.D. Coey, and E. Salje, Eds., Structural and Magnetic Phase Transitions in Minerals. Advances in Physical Geochemistry, 7, 141–161. Springer-Verlag, Berlin.

Ghose, S., Hewat, A.W., Marezio, M., Dang, N.V., Robie, R.A., and Evans, H.T. (1984a) Electron and spin ordering and associated phase transitions in ilvaite, a mixed valence iron silicate. (abstract) Transactions of the American Geophysical Union, 65, 289.

Ghose, S., Hewat, A.W., and Marezio, M. (1984b) A neutron powder diffraction study of the crystal and magnetic structures of ilvaite from 305 K to 5 K—a mixed valence iron silicate with an electronic transition. Physics and Chemistry of Minerals, 11, 67–74.

Ghose, S., Sen Gupta, P.K., and Schlemper, E.O. (1985) Electron ordering in ilvaite, a mixed-valence iron silicate: crystal structure refinement at 138 K. American Mineralogist, 70, 1248–1252.

Ghose, S., Tsukimura, K., and Hatch, D.M. (1989) Phase transitions in ilvaite, a mixed-valence iron silicate. II. A single crystal X-ray diffraction study and Landau theory of the monoclinic to orthorhombic phase transition induced by charge delocalization. Physics and Chemistry of Minerals, 16, 483–496.

Haga, N. and Takéuchi, Y. (1976) Neutron diffraction study of ilvaite. Zeitschrift für Kristallographie, 144, 161–174.

Ibers, J.A. and Hamilton, W.C., Eds. (1974) International Tables for X-ray Crystallography, vol. IV, 366 p. Kynock, Dordrecht, the Netherlands.

Litterst, F.J. and Amthauer, G. (1984) Electron delocalization in ilvaite, a reinterpretation of its ^{57}Fe Mössbauer spectrum. Physics and Chemistry of Minerals, 10, 250–255.

Logan, M.A.V. (2000) Mineralogy and geochemistry of the Gualilán skarn deposit in the Precordillera of Western Argentina. Ore Geology Reviews 17, 113–138.

Lucchetti, G. (1989) High-pressure ilvaite-bearing mineral assemblage from the Voltri group (Italy). Neues Jahrbuch für Mineralogie Monatshefte, 1989, 1–7.

Meinert, L.D. (1987) Skarn zonation and fluid evolution in the Groundhog Mine, Central Mining District, New Mexico. Economic Geology, 82, 523–545.

Naslund, H.R., Hughes, J.M., and Birnie, R.W. (1983) Ilvaite, an alteration product replacing olivine in the Skaergaard intrusion. American Mineralogist, 68, 1004–1008.

Nolet, D.A. and Burns, R.G. (1979) Ilvaite: a study of temperature dependent electron delocalization by the Mössbauer effect. Physics and Chemistry of Minerals, 4, 221–234.

North, A.C.T., Phillips, D.C., and Mathews, F.S. (1968) A semiempirical method of absorption correction. Acta Crystallographica, A24, 351–359.

Plimer, I.R. and Ashley P.M. (1978) Manganoan ilvaite from Broken Hill, N.S.W. and Ban Ban, Queensland, Australia. Mineralogical Magazine, 42, 85–88.

Robie, R.A., Evans, H.T., Jr., and Hemingway, B.S. (1988) Thermophysical properties of ilvaite $CaFe^{2+}_2Fe^{3+}Si_2O_7O(OH)$; heat capacity from 7 to 920 K and thermal expansion between 298 and 856 K. Physics and Chemistry of Minerals, 15, 390–397.

Robinson, K., Gibbs, G.V., and Ribbe, P.H. (1971) Quadratic elongation: A quantitative measure of distortion in coordination polyhedra. Science, 172, 567–570.

Schmidbauer, E. and Amthauer, G. (1998) Study of the electrical charge transform in ilvaite using impedance spectroscopy and thermopower data. Physics and Chemistry of Minerals, 25, 522–533.

Sheldrick, G.M. (1993) SHELXL-93. A new structure refinement program. University of Gottingen, Germany.

Takéuchi, Y., Haga, N., and Bunno, M. (1983) X-ray study on polymorphism of ilvaite, $HCa\ Fe^{2+}_2Fe^{3+}O_2[Si_2O_7]$. Zeitschrift für Kristallographie, 163, 267–283.

Takéuchi, Y., Sawada, H., and Taniguchi, H. (1993) The ilvaite problem. Proceeding of the Inst. of Natural Sciences, Nihon University, 28, 39–43.

Takéuchi, Y., Sawada, H., Taniguchi, H., Uno, R., and Tabira, Y. (1994) Submicroscopic twinning and chemical inhomogeneity of ilvaite, a mixed-valence iron sorosilicate $HCa\ Fe^{2+}_2Fe^{3+}Si_2O_9$. Zeitschrift für Kristallographie, 209, 861–869.

Xuemin, K., Ghose, S., and Dunlap, B.D. (1988) Phase transition in ilvaite, a mixed-valence iron silicate. I. A ^{57}Fe Mössbauer study of magnetic order and spin frustration. Physics and Chemistry of Minerals, 16, 55–60.

Yamanaka, T. and Takéuchi, Y. (1979) Mössbauer spectra and magnetic features of ilvaites. Physics and Chemistry of Minerals, 4, 149–159.

MANUSCRIPT RECEIVED JANUARY 13, 2001
MANUSCRIPT ACCEPTED JANUARY 30, 2002
MANUSCRIPT HANDLED BY M. DARBY DYAR